JOC Article

Colorimetric and Ratiometric Fluorescence Sensing of Fluoride: Tuning Selectivity in Proton Transfer

Xiaojun Peng,*,† Yunkou Wu,† Jiangli Fan,† Maozhong Tian,† and Keli Han*,‡

State Key Laboratory of Fine Chemicals, Dalian University of Technology, 158 Zhongshan Road, Dalian 116012, P. R. China and Dalian Institute of Chemical Physics, Chinese Academy of Sciences, 457 Zhongshan Road, Dalian 116023, P. R. China

pengxj@dlut.edu.cn

Received August 22, 2005

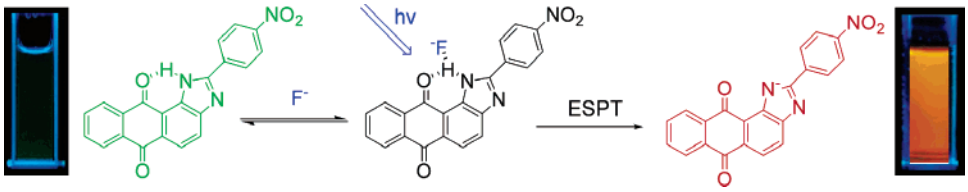

Phenyl-1*H*-anthra[1,2-*d*]imidazole-6,11-dione (**1**) and its derivatives (**2** and **3**) have been investigated as new colorimetric and ratiometric fluorescent chemosensors for fluoride. Acute spectral responses of **1** and **3** to fluoride in acetonitrile have been observed: an approximately 100 nm red shift in absorption and fluorescence emission and a very large ratiometric fluorescent response (R_{max}/R_{min} is 88 for sensor **1** and 548 for sensor **3**). From the changes in the absorption, fluorescence, and ^{1}H NMR titration spectra, proton-transfer mechanisms have been deduced. In ground states, a two-step process has been observed: first, the formation of the sensor-fluoride hydrogen-bond complex $[LH\cdots F]^-$ and then the fluoride-induced deprotonation of the complex to form L^- and FHF^-. In excited states, the excited-state intermolecular proton-transfer made a contribution to the deprotonation. The selectivity for F^- can be tuned by electron push−pull properties of the substituents on the phenyl para position of the sensors. Sensor **1** shows the best selectivity. The excellent selectivity of **1** for F^- is attributed to the fitness in the acidity of its NH-group, which is tuned to be able to distinguish the subtle difference in the affinity of F^-, $CH_3CO_2^-$, and $H_2PO_4^-$ to proton.

Introduction

Considerable efforts have been made to design chemosensors for anions. The reason for this intensive interest is the importance of the detection and quantification of anions in disciplines such as biology and environmental science.[1] Among the interests in biologically functional anions, fluoride is one of particular importance owing to its established role in dental care[2] and treatment of osteoporosis.[3] As the smallest and the most electronegative atom, fluoride has unique chemical properties and can form the strongest hydrogen-bond interaction with hydrogen-bond donors. The major of the reported fluoride sensors are based on colorimetric changes or fluorescent quenchings;[4] few of them experience fluorescence enhancement.[5] Up to now, however, there has been a paucity of reports of fluoride sensors based on the ratiometric fluorescence,[6] the fluorescent emission wavelength changes upon interaction with fluoride.

† Dalian University of Technology.
‡ Chinese Academy of Sciences.

(1) (a) Stibor, I., Ed.; Anion Sensing. *Top. Curr. Chem.* **2005**, *255*. (b) Gale, P. A., Ed.; Special issue: 35 Years of Synthetic Anion Receptor Chemistry. *Coord. Chem. Rev.* **2003**, *240*, 1−2. (c) Martínez-Máñez, R.; Sancenón, F. *Chem. Rev.* **2003**, *103*, 4419−4476. (d) Suksai, C.; Tuntulani, T. *Chem. Soc. Rev.* **2003**, *32*, 192−202. (c) Sessler, J. L.; Davis, J. M. *Acc. Chem. Res.* **2001**, *34*, 989−997. (e) Schmidtchen, F. P.; Berger, M. *Chem. Rev.* **1997**, *97*, 1609−1646.

(2) Kirk, K. L. *Biochemistry of the Halogens and Inorganic Halides*; Plenum Press: New York, 1991; p 58.

(3) Kleerekoper, M. *Endocrinol. Metab. Clin. North Am.* **1998**, *27*, 441.

(4) (a) Black, C. B.; Andrioletti, B.; Try, A. C.; Ruiperez, C.; Sessler, J. L. *J. Am. Chem. Soc.* **1999**, *121*, 10438−10439. (b) Anzenbacher, P., Jr.; Jursikova, K.; Sessler, J. L. *J. Am. Chem. Soc.* **2000**, *122*, 9350−9351. (c) Miyaji, H.; Sessler, J. L. *Angew. Chem., Int. Ed.* **2001**, *40*, 154−157. (d) Furuta, H.; Maeda, H.; Osuka, A. *J. Am. Chem. Soc.* **2001**, *123*, 6435−6436. (e) Yamaguchi, S.; Akiyama, S.; Tamao, K. *J. Am. Chem. Soc.* **2001**, *123*, 11372−11375. (f) Kim, S. K.; Yoon, J. *Chem. Commun*. **2002**, 770−771. (g) Piątek, P.; Jurczak, J. *Chem. Commun*. **2002**, 2450−2451. (h) Jiménez, D.; Martínez-Máñez, R.; Sancenón, F.; Soto, J. *Tetrahedron Lett.* **2002**, *43*, 2823−2825. (i) Gabbaï, F. P.; Solé, S. *Chem. Commun*. **2002**, 1284−1285. (j) Jose, D. A.; Kumar, D. K.; Ganguly, B.; Das, A. *Org. Lett.* **2004**, *6*, 3445−3448. (k) Xu, S.; Chen, K. C.; Tian, H. *J. Mater. Chem.* **2005**, 2676−2680. (l) Cho, E. J.; Ryu, B. J.; Lee, Y. J.; Nam, K. C. *Org. Lett.* **2005**, *7*, 2607−2609.

10.1021/jo051766q CCC: $30.25
Published on Web 11/05/2005

Ratiometric fluorescence measurements[7] can increase the selectivity and the sensitivity of the detection, because the ratio of the fluorescent intensities at two wavelengths is independent of the concentration of the sensor, the fluctuation of source-light intensity, and the sensitivity of instrument. Different kinds of mechanisms have been used to design the ratiometric fluorescent sensors for anions, such as intramolecular charge transfer (ICT),[8a] fluorescence resonance energy transfer (FRET),[8b] excimer/exciplex formation,[8c] luminescent lanthanide-anion complexation,[8d] chemodosimetry,[8e] and anion-sensitive dual chromophore recognization.[8f]

Proton transfer[9] is another mechanism utilized in the design of the ratiometric fluorescent sensor. Hamilton et al.[9a] reported a ratiometric fluorescent $H_2PO_4^-$ sensor based on the macrocyclic amide containing coumarin fluorophore that involves both the excited-state charge transfer and proton-transfer dual channels. More recently, Tian et al.[6b] reported a naphthalimide-containing fluorescent chemosensor for fluoride based on a proton transfer signaling mechanism. However, the detailed mechanisms, in particular, the relation between the ground-state and excited-state proton transfer process existing in the anion recognition, have not been disclosed, and consequently the relationship between the selectivity and the molecular structure is not clear yet.

Recently, based on imidazole ion, biimidazolate diamides, dipyrrolylquinoxalines, indolocarbazoles, calix[4]-pyrrole or its derivatives, and urea or thiourea receptors,[10] various kinds of anion sensors have been developed. In the presence of the anions, the NH-anion hydrogen-bond or anion-induced deprotonation of the NH groups was observed, which resulted in fluorescence quenching by photoinduced electron transfer (PET) mechanism or red shift of the absorption by a charge transfer (CT) mechanism. To gain an insight into hydrogen-bond formation and neat proton-transfer existing in the anion recognition process, Fabbrizzi et al.[11] have investigated various colorimetric anion receptors containing NH binding sites and concluded that the deprotonation trend is enhanced by the increase of the acidity of the hydrogen-bond donors and the basicity of the anions. Because their receptors have no fluorescence, they can only investigate the ground-state receptor-anion interactions.

SCHEME 1. Molecular Structures 1, 2, and 3

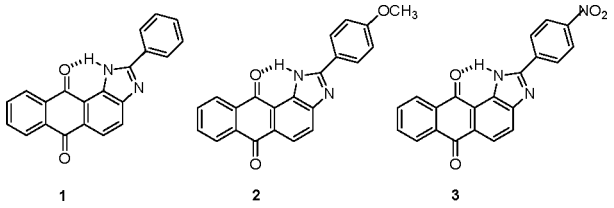

SCHEME 2. Synthesis of 1, 2, and 3

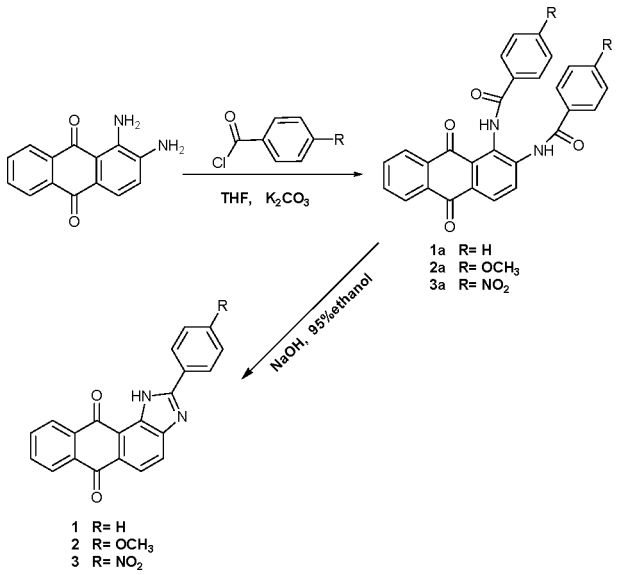

As a fluorophore, phenyl-1*H*-anthra[1,2-*d*]imidazole-6,11-dione (**1**),[12] which possesses the intramolecular hydrogen bonding between the NH (hydrogen-bond donors) of the imidazole ring with the neighboring quinone carbonyl group (hydrogen-bond acceptors), is a new candidate to investigate hydrogen-bond formation and proton-transfer process for the receptor-anion interactions. The intramolecular hydrogen bonding existing between the donors and the acceptors could enhance the acidity of the hydrogen-bond donors.[13]

In the present study, we utilize this intramolecular hydrogen bond in **1** (Scheme 1) as the fluoride binding site and reveal first the selectivity-structure relationship

(5) (a) Cho, E. J.; Moon, J. W.; Ko, S. W.; Lee, J. Y.; Kim, S. K.; Yoon, J.; Nam, K. C. *J. Am. Chem. Soc.* **2003**, *125*, 12376−12377. (b) Xu. G. X.; Tarr, M. A. *Chem. Commun.* **2004**, 1050−1051. (c) Curiel, D.; Cowley, A.; Beer, P. D. *Chem. Commun.* **2005**, 236−238. (d) Thiagarajan, V.; Ramamurthy, P.; Thirumalai, D.; Ramakrishnan, V. T. *Org. Lett.* **2005**, *7*, 657−660.

(6) (a) Kubo, Y.; Yamamoto, M.; Ikeda, M.; Takeuchi, M.; Shinkai, S.; Yamaguchi, S.; Tamao, K. *Angew. Chem., Int. Ed.* **2003**, *42*, 2036−2040. (b) Liu, B.; Tian, H. *J. Mater. Chem.* **2005**, 2681−2686.

(7) Valeur, B. *Molecular Fluorescence: Principles and Applications*; Wiley-VCH: Weinheim, 2002.

(8) (a) Wen, Z. C.; Jiang, Y. B. *Tetrahedron* **2004**, *60*, 11109−11115. (b) Thomas, K.; George, J. A. *Neuron* **2000**, *27*, 447−459. (c) Nishizawa, S.; Kato, Y.; Teramae, N. *J. Am. Chem. Soc.* **1999**, *121*, 9463−9464. (d) Yann, B.; Martin, J. C.; David, P.; Rachel, S. *Chem. Commun.* **2002**, 1930−1931. (e) Ramachandram, B.; Joseph, R. L.; Chris, D. G. *Anal. Biochem.* **2004**, *327*, 82−90. (f) Jayaraman, S.; Biwersi, J.; Verkman, A. S. *Am. J. Physiol.* **1999**, *276*, 747−757.

(9) (a) Choi, K.; Hamilton, A. D. *Angew. Chem., Int. Ed.* **2001**, *40*, 3912−3915. (b) Tong, H.; Zhou, G.; Wang, L.; Jing, X.; Wang, F.; Zhang, J. *Tetrahedron Lett.* **2003**, *44*, 131−134. (c) Zhang, X.; Guo, L.; Wu, F. Y.; Jiang, Y. B. *Org. Lett.* **2003**, *5*, 2667−2670.

(10) (a) Ihm, H.; Yun, S.; Kim, H. G.; Kim, J. K.; Kim, K. S. *Org. Lett.* **2002**, *4*, 2897−2900. (b) Yun, S.; Ihm, H.; Kim, H. G.; Lee, C. W.; Indrajit, B.; Oh, K. S.; Gong, Y. J.; Lee, J. W.; Yoon, J.; Lee, H. C.; Kim, K. S. *J. Org. Chem.* **2003**, *68*, 2467−2470. (c) Chellappan, K.; Singh, N. J.; Hwang, I. C.; Lee, J. W.; Kim, K. S. *Angew. Chem., Int. Ed.* **2005**, *44*, 2899−2903. (d) Causey, C. P.; Allen, W. E. *J. Org. Chem.* **2002**, *67*, 5963−5968. (e) Gale, P. A.; Anzenbacher, J. P.; Sessler, J. L. *Coord. Chem. Rev.* **2000**, *222*, 57−102. (f) Bondy, C. R.; Loeb, S. J. *Coord. Chem. Rev.* **2003**, *240*, 77−99. (g) Camiolo, S.; Gale, P. A.; Hursthouse, M. B.; Light, M. E. *Org. Biomol. Chem.* **2003**, *1*, 741−744. (h) Gunnlaugsson, T.; Davis, A. P.; Hussey, G. M.; Tierney, J.; Glynn, M. *Org. Biomol. Chem.* **2004**, *2*, 1856−1863.

(11) (a) Boiocchi, M.; Del Boca, L.; Gómez, D. E.; Fabbrizzi, L.; Licchelli, M.; Monzani, E, *J. Am. Chem. Soc.* **2004**, *126*, 16507−16514. (b) Gómez, D. E.; Fabbrizzi, L.; Licchelli, M.; Monzani, E. *Org. Biomol. Chem.* **2005**, *3*, 1495−1500. (c) Amendola, V.; Boiocchi, M.; Fabbrizzi, L.; Palchetti, A. *Chem. Eur. J.* **2005**, *11*, 120−127. (d) Boiocchi, M.; Del Boca, L.; Gómez, D. E.; Fabbrizzi, L.; Licchelli, M.; Monzani, E. *Chem. Eur. J.* **2005**, *11*, 3097−3104. (e) Gómez, D. E.; Fabbrizzi, L.; Licchelli, M. *J. Org. Chem.* **2005**, *70* (14), 5717−5720.

(12) (a) Yoshida, K.; Yamasaki, J.; Tagashira, Y.; Watanabe, S. *Chem. Lett.* **1996**, 9−10. (b) Yoshida, K.; Mori, T.; Watanabe, S.; Kawai H.; Nagamura, T. *J. Chem. Soc., Perkin Trans. 2* **1999**, 393−397. (c) Kawai, H.; Nagamura, T.; Mori, T.; Yoshida, K. *J. Phys. Chem. A* **1999**, *103*, 660−664.

(13) Chen, X.; Walthall, D. A.; Brauman, J. I. *J. Am. Chem. Soc.* **2004**, *126*, 12614−12620.

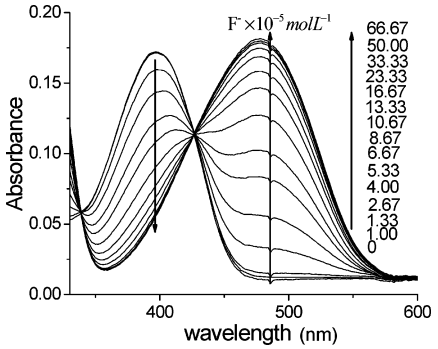

FIGURE 1. Change in UV−vis spectra for **1** (1.0×10^{-5} M) in CH_3CN with the addition of $[(Bu)_4N]F$.

by tuning the acidity and the hydrogen-bond donor property of the NH moiety with *p*-OCH_3 electron-donating derivative **2** and *p*-NO_2 electron-attracting derivative **3**. From the absorption titration spectra, ^1H NMR titration experiments and fluorescence titration spectra, the detail processes of the ground-state and excited-state proton-transfer present in the anion recognition have been disclosed. Also, the sensors show the largest signal/noise ratio (R_{max}/R_{min}) in the ratiometric fluorescent fluoride sensors that have ever reported.

Results and Discussion

Synthesis. Using the synthesis methods described previously,[12] we could not obtain satisfactory product yields.

The synthesis of these sensors is improved by following the methodology shown in Scheme 2. In the first step, the mixtures of 1,2-diaminoanthraquinone and the corresponding benzoyl chloride were refluxed in THF for 10 h to give the α,*β*-disubstituted acylation intermediates. Then the acylation products were condensed to form sensors by refluxing in 95% ethanol in the presence of sodium hydroxide. The structures of sensors were characterized on the basis of ^1H and ^{13}C NMR and HRMS. The ^1H NMR spectra (in DMSO-d_6) exhibiting a broad singlet signal at around δ_H 11−14 ppm support the formation of intramolecular hydrogen bonding between the NH of the imidazole ring and the neighboring quinone carbonyl group.

UV−vis Spectral Responses of 1. The interaction of sensor **1** with anions was investigated through spectrophotometric titrations by adding a standard solution of the tetrabutylammonium salt of anions to a dry CH_3CN solution of sensor. Figure 1 shows the UV−vis spectral changes of **1** during the titration with fluoride ions. Upon addition of 1 molar equiv of fluoride ions, little change was observed and care was taken to avoid the contamination by the water in preparation of the solution and during titration. However, with the addition of a further amount of fluoride ions, the peak at the λ_{max}^{ab} of 384 nm, the $\pi-\pi^*$ transition of the chromophore, disappears gradually, and a new band forms at 479 nm, which is the charge transfer (CT) band. The yellow color of the sensor solution turns red at the same time. Though the isosbestic points are 339 and 427 nm, respectively, the stoichiometry of the **1**-fluoride interaction was confirmed to be 1:2 from the Job plot (Figure S1). Analogous

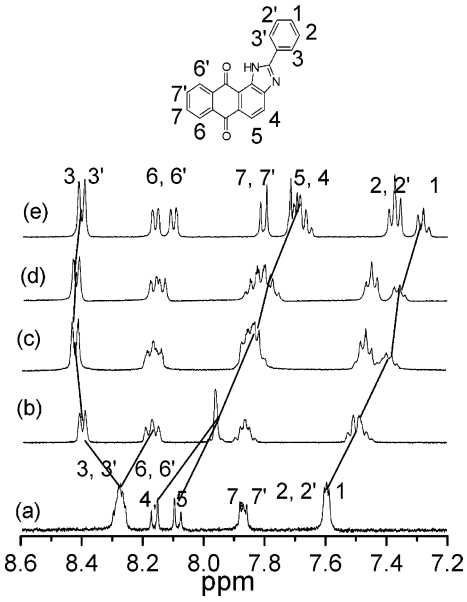

FIGURE 2. Partial ^1H NMR (400 MHz) spectra of **1** (1.0×10^{-2} M) in CD_3CN in (a) the absence and the presence of (b) 1.0, (c) 3.0, (d) 5.0, and (e) 10.0 equiv of $[(Bu)_4N]F$.

investigations were carried out on a variety of anions such as $CH_3CO_2^-$, $H_2PO_4^-$, HSO_4^-, Cl^-, and Br^-. Only $CH_3CO_2^-$ and $H_2PO_4^-$ induced some spectral changes, but the spectral responses were not as sensitive as fluoride with the increase of anion concentrations. Other anions such as HSO_4^-, Cl^-, and Br^- did not induce any spectra response.

^1H NMR Titration and Two-Step Mechanism. ^1H NMR titration experiments in CD_3CN were conducted to look into the nature of the new peak formed in UV−vis fluoride titration spectra. For the ^1H NMR spectrum, two effects are responsible for the ^1H NMR changes upon NH-fluoride hydrogen-bond formation:[11a] (1) through-bond effects, which increase the electron density of the phenyl ring and promote an upfield shifts, and (2) through-space effects, which polarize C−H bond in proximity to hydrogen bond, create partial positive charge on the proton, and cause a downfield shifts. As shown in the partial ^1H NMR fluoride titration spectra of **1** in Figure 2. Upon addition of 1 molar equiv of fluoride ions, the downfield shift of protons 3 and 3′ is observed, which is ascribed to the through-space effects, the polarization C−H bond in proximity to the hydrogen bond. This indicates the formation of a hydrogen-bond complex at this stage. With the addition of a further amount of fluoride ions, the protons 3 and 3′ almost do not change, while the phenyl protons adjacent to imidazole ring, especially for proton 1, shift upfield significantly, which indicates the increase of the electron density on the phenyl ring owing to the through-bond effects. This indicates the deprotonation of the NH group of the imidazole ring. The deprotonation can be directly observed in the NMR titration spectra in DMSO-d_6 (Figure 3), which is a more polar solvent with a stronger deprotonation ability than CD_3CN.[11e] In Figure 3, the majority of signals on the phenyl rings shift upfield distinctly after the addition of 1 molar equiv of fluoride ions owing to the through-bond effects, and the complete disappearance of the signals for the NH protons (13.2 ppm) was also observed at the same time. Interestingly,

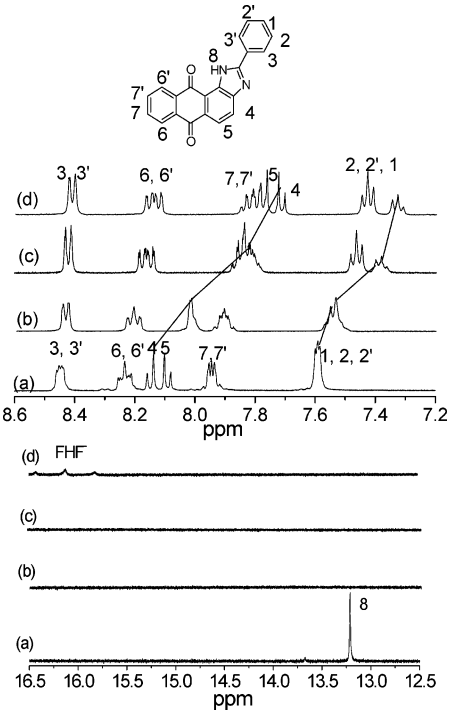

FIGURE 3. Partial ^{1}H NMR (400 MHz) spectra of **1** (1.0×10^{-2} M) in DMSO-d_6 in (a) the absence and the presence of (b) 1.0, (c) 3.0, and (d) 5.0 equiv of $[(Bu)_4N]F$.

after the addition of 5 molar equiv of fluoride ions, a new 1:2:1 triplet signal at 16.2 ppm appears, which is ascribed to the FHF^- dimer.[11a,14] The existence of this new species indicates the deprotonation of the NH group. The absence of the NH proton for free **1** and FHF^- dimer signal in the excess of fluoride ions in CD_3CN (Figure 2) is ascribed to the occurrence of a fast proton exchange with water that is present in solution as impurity. This deprotonation process is also confirmed by the identical UV−vis spectral changes observed in the titration experiment with tetrabutylammonium hydroxide as that of with fluoride ions (Figure S2). With the deprotonation of **1**, charge delocalizes on the entire conjugated system, which shifts the phenyl rings upfield further. From the result of ^{1}H NMR titration, it is found that **1** and fluoride form the hydrogen-bond complex upon addition of **1** molar equiv of fluoride ions, while the UV−vis spectra have almost no changes at the same time; with the increase of the fluoride concentrations, a new deprotonated species appears, and the CT bond of UV−vis spectra forms quickly. These results suggest that sensor-fluoride interaction is indeed a two-step process shown in Scheme 3: at low fluoride concentration, sensor-fluoride interaction is the authentic hydrogen binding, and with the increase of the fluoride ions, excess fluoride interact with the sensor-fluoride complex and induce the deprotonation of the sensor.

***K*$_d$ from Absorption Spectra.** The two-step process agrees well with the Fabbrizzi paradigm for anion-induced urea deprotonation that produced stepwise colorimetric changes.[11] So we made use of the equilibrium they have developed to investigate our system. In particular, the following two equilibria can express the processes shown in Scheme 3:

$$LH + X^- \overset{K_a}{\rightleftharpoons} [LH\cdots X]^- \quad (1)$$

$$[LH\cdots X]^- + X^- \overset{K_d}{\rightleftharpoons} L^- + [HX_2]^- \quad (2)$$

Equation 1 gives the association constant K_a and stands for a genuine hydrogen-bond formation. Equation 2 gives the dissociation constant K_d and stands for an anion-induced deprotonation process. In the first step, sensor-anion hydrogen-bond formation produces minimal disturbance on the dipole associated with the charge-transfer transition of sensor **1** and consequently only a small change was observed in the spectra (Figure 1). Then the second step produces a deprotonation species. With the charge redistribution taking place within the deprotonated species, the UV−vis spectra exhibit a red shifted CT band. From the results of UV−vis titration spectra, all anions investigated experience the first step; only the more basic anion F^-, $CH_3CO_2^-$, and $H_2PO_4^-$ can undergo the second step.

Because of the small UV−vis spectral changes upon addition of the 1 molar equiv of fluoride ions, it is impossible to calculate the log $K_a{}^a$ from UV−vis titration spectra. However, log $K_d{}^a$ (Table 1) can be obtained from the spectral changes. The log $K_d{}^a$ showing the selectivity of **1** to the anions has the order $F^- > CH_3CO_2^- > H_2PO_4^-$. As the changes in UV−vis spectra associate with the ground state of the sensors, the log $K_d{}^a$ of sensor-anion interaction compiled in Table 1 are the ground-state dissociation constants.

By combining the eq 1 and eq 2, the overall equilibrium can be obtained:

$$LH + 2X^- \rightleftharpoons L^- + [HX^2]^- \quad (3)$$

Equation 3 can also be combined with the following two equilibria:

$$LH \rightleftharpoons L^- + H^+ \quad (4)$$

$$H^+ + 2X^- \rightleftharpoons [HX_2]^- \quad (5)$$

So the overall constant of eq 3, K_3, can be expressed as follows:

$$K_3 = K(LH)_{\text{dissociation}} \times K([HX_2]^-)_{\text{association}} \quad (6)$$

Equation 6 suggests two factors make contributions to the deprotonation process: the acidity of the hydrogen-bond donors and the thermal stabilization of XHX^- dimer. The high selectivity for fluoride is not only due to the strong hydrogen-bond ability and the basic nature of fluoride ions in organic solution but also due to the particular high stability of the FHF^- dimer, for which the highest hydrogen bond energy in the gas phase has been calculated.[15]

Tuning the Acidity of the NH Group. A resonance structure of the deprotonated form of **1** (Scheme 4) shows that the electron density of the phenyl para position is enhanced upon deprotonation. This indicates the acidity

(14) Descalzo, A. B.; Rurack, K.; Weisshoff, H.; Martínez-Máñez, R.; Marcos, M. D.; Amorós, P.; Hoffmann, K.; Soto, J. *J. Am. Chem. Soc.* **2005**, *127*, 184−200.
(15) Gronert, S. *J. Am. Chem. Soc.* **1993**, *115*, 10258−10266.

SCHEME 3. Stepwise Changes for 1 and Fluoride Interaction

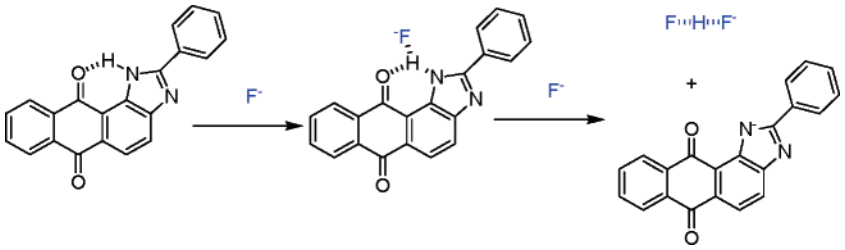

TABLE 1. Proton-Dissociation Constants (log K_d) of 1 Interaction with Anions[a]

anion	log K_d[a]	log K_d[#]
F^-	3.92 ± 0.07	4.61 ± 0.08
$CH_3CO_2^-$	3.35 ± 0.03	3.90 ± 0.07
$H_2PO_4^-$	1.48 ± 0.12	1.96 ± 0.09

[a] From UV−vis titration spectra. [#] From fluorescence titration spectra.

SCHEME 4. Resonance Representation of the Deprotonated Form of 1

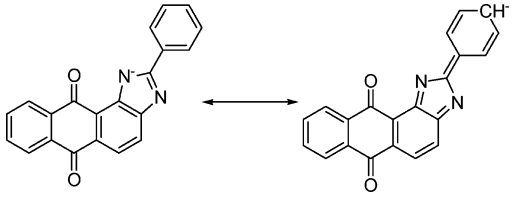

of this kind of sensors can be tuned by changing the electron property of the substituent on the para position.

So **2** (p-OCH_3 electron-donating substituent) and **3** (p-NO_2 electron-withdrawing substituent) were synthesized to investigate the effect of electron properties of p-substituent on the hydrogen-bond property and fluoride selectivity. As expected, UV−vis fluoride titration spectra of **2** indeed exhibit stepwise changes (Figure 4). First, the λ_{max}^{ab} at 416 nm of **2** almost do not change until the addition of a very large amount (up to 233 molar equiv) of fluoride ions; this step assigns to the **2**-fluoride hydrogen-bond formation. Second, further addition of fluoride induces the production of the deprotonated species. $CH_3CO_2^-$ induced similar two-step changes, but other anions including $H_2PO_4^-$ only experienced the first step change. The introduction of the electron-donating group can enhance the electron density of the imidazole ring and consequently increase the basicity of the hydrogen-bind donors, so the deprotonation becomes more difficult.

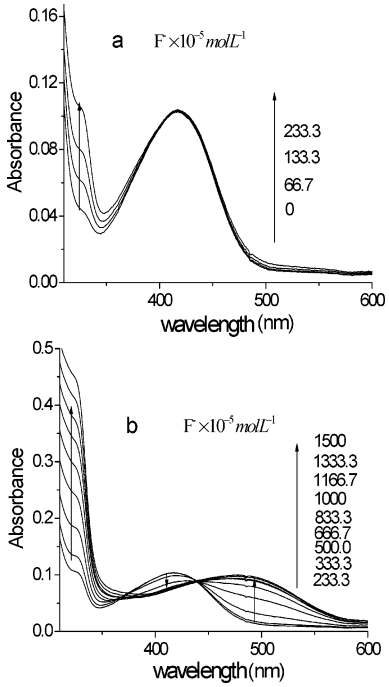

FIGURE 4. Change in UV−vis spectra for **2** (1.0×10^{-5} M) in CH_3CN with the addition of $[(Bu)_4N]F$ (a) from 0 to 233.3 equiv and (b) from 233.3 to 1500 equiv.

As for the $-NO_2$ electron-attracting substituent derivative **3**, it also experiences spectral changes (from 380 to 497 nm) upon interaction with fluoride. Compared with those of **1** and **2**, the fluoride titration spectra of **3** take on the significant CT band upon addition of 1 molar equiv of fluoride ions (Figure 5a). This result indicates the strong electron-withdrawing p-NO_2 substituent makes the charge delocalization more easily upon interaction with fluoride. With the Specfit program,[16] best fits of the UV−vis titration spectra give the log $K_a^a = 5.61 \pm 0.06$ and log $K_d^a = 4.83 \pm 0.06$ for the two-step changes. The corresponding species distribution diagram for this two-step process is presented in Figure 5b. Upon addition of the fluoride, the sensor-anion hydrogen-bond complex LH···F^- forms first and reaches the maximum concentration with the added fluoride ions in the range of 1−2 molar equiv, while the deprotonated form L^- appears shortly after the LH···F^- and increases quickly with the consumption of the LH and LH···F^- species. The solution almost contains only the LH···F^- and L^- after added fluoride up to 7 molar equiv and the L^- increases gradually with the decrease of the LH···F^-. For other anions, $CH_3CO_2^-$ and $H_2PO_4^-$ also induce similar spectral changes, but HSO_4^-, Cl^-, and Br^- did not produce any spectral responses.

From the trend of the UV−vis titration spectral changes discussed above, it is found that the electron properties of substituents on the phenyl para position correlate well with the spectral stepwise changes. At this point, it also should be noted that one step of the Brönsted acid−base reaction can proceed between the strong acid and strong base. So by increasing the electron-attracting ability of substituent at the phenyl para position, sensor-fluoride interactions can experience from two-step complex-deprotonation to one-step Brönsted acid−base reaction transformation. Especially for **3**,

(16) Specfit/32 for Windows: http://www.bio-logic.fr/rapid-kinetics/specfit/Index.html.

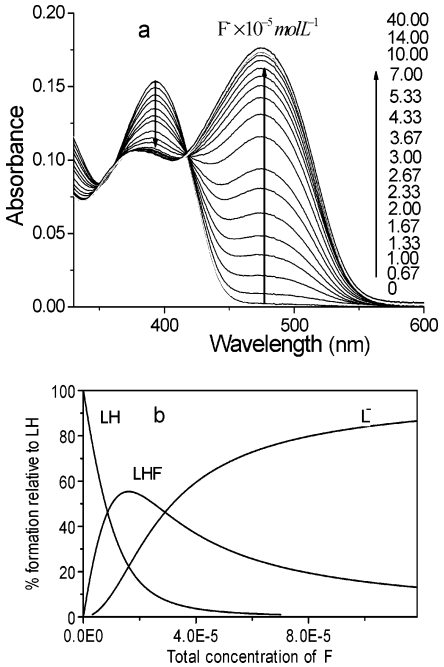

FIGURE 5. (a) Change in UV−vis spectra for **3** (1.0×10^{-5} M) in CH_3CN with the addition of $[(Bu)_4N]F$. (b) The corresponding distribution diagram of the species present at the equilibrium.

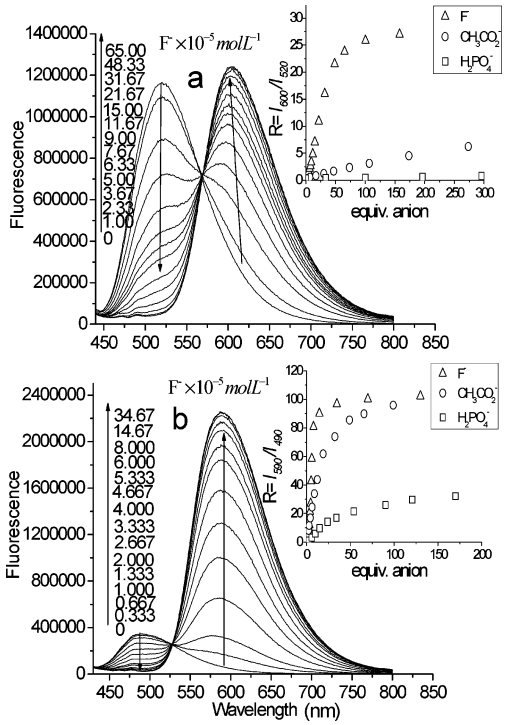

FIGURE 6. Change in fluorescent spectra (uncorrected) for sensors (1.0×10^{-5} M) in CH_3CN upon the addition of a standard solution of $[(Bu)_4N]F$. (a) **1** with the excitation wavelength of 427 nm (isosbestic wavelength). Insert: the corresponding ratiometric plot of I_{600}/I_{520} versus equivalents of fluoride. (b) **3** with the excitation wavelength of 418 nm (isosbestic wavelength). Insert: The corresponding ratiometric plot of I_{590}/I_{490} versus equivalents of fluoride.

the following acid−base reaction eq 7 maybe also takes place upon the presence of fluoride besides **3**-fluoride hydrogen-bond complex formation in the ground state.

$$LH + X^- \rightarrow L^- + HX \qquad (7)$$

Ratiometric Fluorescence Responses. Spectrofluorimetric titrations were also investigated in CH_3CN. The fluorescence responses of the interaction of **1** with fluoride ions were recorded with an excitation at the isosbestic point of 427 nm (Figure 6a). The free **1** exhibits an emission maximum at 520 nm, while the emission maximum shifts to 600 nm after the addition of fluoride ions and a well-defined isoemission point at 568 nm is observed. The emission intensity ratio, I_{600}/I_{520}, increases with the increase in the fluoride concentrations, which allows the detection of fluoride ions ratiometrically. Among the anions investigated, only $CH_3CO_2^-$ and $H_2PO_4^-$ induced similar spectral changes, but the ratiometric responses were not as sensitive as with F^-. The dissociation constants from fluorescence titration, $\log K_d^{\#}$, of **1** with different anions (Table 1) show that the selectivity of **1** for F^- ion is 5-fold larger than that for $CH_3CO_2^-$ and 440-fold than that for $H_2PO_4^-$. The excellent selectivity of **1** for F^- over $CH_3CO_2^-$ is attributed to the fitness in the acidity of its NH-group.

Different from **1**, the fluorescence fluoride titration spectra of **2** also displays stepwise changes (Figure S3): the fluorescence increases slightly with the addition of fluoride, and then a fluorescence-quenched deprotonation band develops with the excess of fluoride. As for **3**, though its fluoride selectivity is not as good as for **1** (Figure S4), it exhibits more efficient fluorescence responses during the interaction with fluoride (Figure 6b).

TABLE 2. Ratio of the Sensor Quantum Yields (ϕ_r) and the *R* Values (R_r) of the Solutions Containing Sensors in the Presence of Excess of Anions to Solutions in the Absence of Anions

anion	**1**ϕ_r [a]	**3**ϕ_r [a]	**1**R_r [b]	**3**R_r [b]
F^-	2.7	18.0	88	548
$CH_3CO_2^-$	2.5	18.0	32	548
$H_2PO_4^-$	2.0	16.0	7	178

[a] The quantum yield of free **1** is 0.019 and free **3** is 0.006, and the quinine sulfate with the quantum yields of 0.51 in sulfuric acid (0.05 M) was used as the standard for quantum yield measurements. [b] R_r is the R_{max}/R_{min} determined at the wavelengths shown in Figure 6.

The ratio of the limiting values R_r (Table 2) in the absence and excess of anions, R_{max}/R_{min}, reflecting the limiting dynamic range and resolution for concentration measurements,[17] is a decisive parameter for comparing the performance of sensors. To our knowledge, R_r values of **1** (88) and **3** (548) listed in Table 2 are the largest signal/noise ratio in the ratiometric fluorescent fluoride sensors that have ever been developed.

From the fluorescent ratiometric responses discussed above, it is found that the electron property of the substituent on the phenyl para position can influence the fluorescence properties of the deprotonated species: the stronger the electron-attracting ability of the substituents, the larger the fluorescence enhancement for the

(17) Henary, M. M.; Wu, Y. G.; Fahrni, C. J. *Chem. Eur. J.* **2004**, *10*, 3015−3025.

deprotonated sensors but the less fluoride selectivity. By tuning the acidity of the NH-group with the different substituents, both the best selectivity and sensitivity might be obtained.

Excited-State Intermolecular Proton Transfer. It has been known that excited-state intramolecular proton transfer (ESIPT) exists in 1,5-dihydroxyanthraquinone and some 1-(acylamino)anthraquinones,[18] which possess dual fluorescence emissions: short-wavelength emission (SWE) for the normal structure and long-wavelength emission (LWE) for the tautomer structure. As **1**, **2**, and **3** did not exhibit LWE by changing solvent polarity or donicity, no ESIPT proceeded in this kind of sensor in the absence of anions. While some NH-containing heteroaromatics are more acidic in their lowest excited singlet states than in their ground states as a result of the occurrence of the excited-state intermolecular proton transfer (ESPT) from the proton donors to proton acceptors[19] and consequently will display larger dissociation constants of proton in excited states than those in their ground states after interaction with proton acceptors such as anions, in fact the existence of the ESPT processes complicates the determinations of the ground-state dissociation constants with fluorescence measurement because of the dependence of fluorescence on the acid−base chemistry of excited-state as well as ground-state.[20a] Interferences from the excited-state reaction can be eliminated if the fluorimetric titration is performed at the isoemissive point.[20b]

When the fluorimetric titration is performed with the excitation wavelength at the isosbestic point, the inflection point of the titration curve is neither the correct value of ground-state log K_d nor the value of excited-state log K_d*, but the coaction result of the log K_d and the log K_d*.[20b] We define the coaction dissociation constant as the apparent dissociation constant log $K_d^{\#}$, and the value of log $K_d^{\#}$ lies just between the log K_d and the log K_d*. So by simply comparing the titration results from the absorption spectra and fluorescence spectra, whether the sensor-anion excited-state intermolecular proton-transfer processes take place can be deduced

In the case of **1**, however, log K_d^{a} of ground state from absorption titration (such as 3.92 ± 0.07 for F^-) are smaller than those of log $K_d^{\#}$ from the fluorescence titration (such as 4.61 ± 0.07 for F^-) (Table 1). This implies that the ESPT takes place indeed and makes a contribution to the deprotonation.

In fact, the photoinduced intermolecular proton transfer can proceed by two different mechanisms:[21] via hydrogen-bonded ground-state complex (binding-excitation-deprotonation, eqs 9 and 10) and with dynamic reaction involving mutual diffusion of the donors and acceptors (excitation-collision-deprotonation: eq 8, eq 11 or 12). The entire processes are shown:

Excitation:

$$\mathrm{LH} \xrightarrow{h\nu} \mathrm{LH}^* \tag{8}$$

$$[\mathrm{LH}\cdots\mathrm{X}]^- \xrightarrow{h\nu} [\mathrm{LH}\cdots\mathrm{X}]^-* \tag{9}$$

Anion-assisted deprotonation:

$$[\mathrm{LH}\cdots\mathrm{X}]^-* \xrightarrow{k_{\mathrm{ESPT1}}} \mathrm{L}^-* + \mathrm{HX} \tag{10}$$

$$\mathrm{LH}^* + \mathrm{X}^- \xrightarrow{k_{\mathrm{ESPT2}}} \mathrm{L}^-* + \mathrm{HX} \tag{11}$$

$$[\mathrm{LH}\cdots\mathrm{X}]^-* + \mathrm{X}^- \xrightarrow{k_{\mathrm{ESPT3}}} \mathrm{L}^-* + \mathrm{XHX}^- \tag{12}$$

Fluorescence:

$$\mathrm{LH}^* \xrightarrow{k_{\mathrm{f1}}} \mathrm{LH} + h\nu_{\mathrm{SWE}} \tag{13}$$

$$\mathrm{L}^-* \xrightarrow{k_{\mathrm{f2}}} L^- + h\nu_{\mathrm{LWE}} \tag{14}$$

First, free sensor LH or sensor-anion complex $[LH\cdots X]^-$ is excited to its excited states LH* (eq 8) or $[LH\cdots X]^-$* (eq 9). Then ESPT takes place in the case of $[LH\cdots X]^-$* and produces the excited deprotonation species L^-* (eq 10), which is presumed to be the fastest process. Another pathway involves the diffusion and encounter of the anion X^- with LH* or $[LH\cdots X]^-$*, which then undergoes ESPT (eq 11 or eq 12), which is generally a diffusion-controlled process. In the case of **3**, the best fits of the fluorescence titration spectra for **3**-fluoride interactions give the log $K_a^{\#}$ = 6.58 ± 0.10 and log $K_d^{\#}$ = 4.86 ± 0.07 with the Specfit program. The log $K_a^{\#}$ calculated from the fluorescence titration is almost 1 unit larger than that from absorption titration (log K_a^{a} = 5.61 ± 0.06), which indicates the ESPT process of eq 10 or eq 11 takes action. The identical value of the log K_d from the two titrations (log K_d^{a} = 4.83 ± 0.06 and log $K_d^{\#}$ = 4.86 ± 0.07) suggests the process represented by eq 12 did not occur. At last, the excited species LH* and L^-* can decay by nonradiative processes to produce heat or by fluorescence emission to generate the SWE and LWE, respectively.

The ESPT in this kind of fluoride chemosensors is also influenced by the electron properties of *p*-substituents on the phenyl ring. The electron-attracting substituents will increase the excited-state acidity and consequently the easiness of releasing the HX from the excited hydrogen-bond complexes (eq 10) or the encounters (eq 11). So the ESPT proceeds more easily in **1** and **3**. Because of the lower acidity of **2**, the deprotonation becomes more difficult not only in the ground state but also in the excited states.

When the imidazole moieties are deprotonated, charge redistribution takes place within the molecules. The deprotonated push−pull chromophores are responsible for a shift in both absorption (color changing from yellow to red) and fluorescence (fluorescence changing from green to red) (Figure 7). With the elimination of the intramolecular hydrogen bonding that associates with the rapid internal conversion,[18a] the quantum yields of the deprotonated species of **1** and **3** increase 2.7- and 18-fold (Table 2) as compared with the free sensors **1** and **3**,

(18) Flom, S. R.; Barbra, P. F. *J. Phys. Chem.* **1985**, *89*, 4489−4494 (b) Smith, T. P.; Zaklika, K, A.; Thakur, K.; Barbra, P. F. *J. Am. Chem. Soc.* **1991**, *113*, 4035−4036.

(19) Schulman, S. G. Acid−Base Chemistry of Excited Singlet States. In *Modern Fluorescence Spectroscopy*; Wehry, E. L., Ed.; Plenum Press: New York, 1976; pp 239−275.

(20) (a) Rosenberg, L. S.; Simons, J.; Schulman, S. G. *Talanta* **1979**, *26,* 867−871. (b) Kowalczyk, A.; Boens, N.; Van den Bergh, V.; De Schryver, F. C. *J. Phys. Chem.* **1994**, *98*, 8585−8590.

(21) (a) Tolbert, L. M.; Nesselroth, S. M. *J. Phys. Chem.* **1991**, *95*, 10331−10336. (b) Lawrence, M.; Marzzacco, C. J.; Morton, C.; Schwab, C.; Halpern, A. M. *J. Phys. Chem.* **1991**, *95*, 10294−10299.

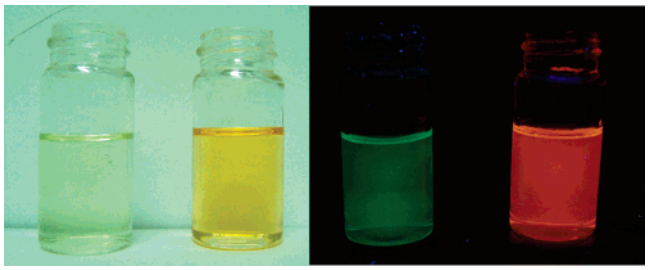

FIGURE 7. Color and fluorescence changes of compound **1** in CH_3CN (5.0×10^{-5} M) after addition of 50 equiv of $[(Bu)_4N]F$. Left to right: **1**, **1** + $[(Bu)_4N]F$, **1** (emission), and **1** + $[(Bu)_4N]F$ (emission). Irradiation at 365 nm using UV lamp.

respectively, which result in the large R_r values for **1** (88) and **3** (548).

Conclusions

In conclusion, we have presented a new kind of colorimetric and ratiometric fluorescent chemosensors for fluoride. The colorimetric and ratiometric properties of these sensors are ascribed to the anion-induced proton transfer. By changing the electron properties of substituents on the phenyl para position, the sensor-fluoride interaction mechanism, the fluoride selectivity, and the fluorescence response can be finely tuned. Generally fluorescent sensors for fluoride ions cannot tell F^- from $CH_3CO_2^-$. The excellent selectivity of **1** for F^- over $CH_3CO_2^-$ is attributed to the fitness in the acidity of its NH-group, which can distinguish the subtle difference in the affinity of F^- and $CH_3CO_2^-$ with proton. The correlation between the electron properties of substituent and the selectivity and the fluorescence responses will be a very useful clue to design more selective chemosensors to recognize F^- in the presence of $CH_3CO_2^-$ and other anions.

Experimental Section

Synthesis and Characterization of 1 and 2. Synthesis of *N*-(1-Phenylamino-9,10-dioxo-9,10-dihydro-anthracen-2-yl)-benzamide (1a). A solution of benzoyl chloride (560 mg, 4 mmol) in THF (10 mL) was added dropwise to a solution of 1,2-diaminoanthraquinone (238 mg, 1 mmol) and K_2CO_3 (345 mg, 2.5 mmol) in THF (70 mL) with stirring at reflux. After being stirred for 12 h, the solvent was removed by evaporation, and the residue was diluted with 20 mL of 2 N sodium carbonate and extracted with dichloromethane. The organic phase was washed with brine, dried over K_2CO_3, filtered, and evaporated to dryness. The crude compound was purified by flash column chromatography on silica gel (10:1 dichloromethane/EtOAc) to afford a yellow solid (347 mg, 78%). δ_H (400 MHz; DMSO-d_6; Me_4Si): 7.3 (t, 2H, J = 7.2 Hz), 7.59−7.70 (m, 4H), 7.91−7.93 (m, 4H), 8.12−8.20 (m, 4H), 8.28 (d, 1H, J = 8.8 Hz), 8.47 (d, 1H, J = 8.8 Hz), 10.19 (s, 1H), 10.83 (s, 1H). δ_C (400 MHz; DMSO-d_6; Me_4Si): 125.2, 126.0, 126.7, 126.8, 127.0, 127.2, 127.5, 128.4, 128.5, 129.4, 129.9, 130.3, 131.9, 132.0, 133.5, 133.7, 133.9, 134.0, 134.2, 139.1, 163.3, 164.9, 166.1, 168.9, 181.2, 183.9. HRMS *m/z* (TOF MS ES$^-$) calcd for $C_{28}H_{17}N_2O_4^-$ ([M − H]$^-$), 445.1188, found, 445.1187.

Synthesis of 2-Phenyl-1*H*-anthra[1,2-*d*]imidazole-6,11-dione (1). A mixture of the compound **1a** (223 mg, 0.5 mmol) and NaOH (20 mg, 0.5 mmol) in 95% ethanol (150 mL) was heated under reflux with stirring for 3 h. After cooling to room temperature, the reaction mixture was neutralized with aqueous HCl, then the solvent was removed by evaporation, and the residue was diluted with 20 mL of 2 N sodium carbonate and extracted with dichloromethane. The organic phase was washed with brine, dried over K_2CO_3, filtered, and evaporated to dryness. The crude compound was purified by flash column chromatography on silica gel (5:1 dichloromethane/EtOAc) to afford a yellow solid (101 mg, 62%). δ_H (400 MHz; DMSO-d_6; Me_4Si): 7.58−7.60 (m, 3H), 7.94 (t, 2H, J = 6.0 Hz), 8.09 (d, 1H, J = 8.0 Hz), 8.14 (d, 1H, J = 8.0 Hz), 8.21−8.25 (m, 2H), 8.44 (m, 2H), 13.22 (s, 1H). δ_C (400 MHz; DMSO-d_6; Me_4Si): 118.0, 122.1, 125.7, 126.5, 127.2, 127.6, 128.6, 129.4, 131.6, 133.1, 133.3, 133.8, 133.9, 134.5, 136.2, 149.4, 156.7, 180.9, 182.6, 185.1. HRMS *m/z* (TOF MS ES$^-$) calcd for $C_{21}H_{11}N_2O_2^-$ ([M − H]$^-$), 323.0821, found, 323.0835.

Synthesis of 2-(4-Methoxyl-phenyl)-1*H*-anthra[1,2-*d*]-imidazole-6,11-dione (2). Using the method described above, the α,β-substituted acylation intermediate was condensed to **2** directly without purification, and the crude compound **2** was purified by flash column chromatography on silica gel (5:1 dichloromethane/EtOAc) to afford a yellow solid (50%). δ_H (400 MHz; DMSO-d_6; Me_4Si): 5.32 (s, 3H), 7.05 (d, 2H, J = 8.8 Hz), 7.78 (m, 2H), 8.04 (d, 1H, J = 8.4 Hz), 8.07 (d, 2H, J = 8.8 Hz), 8.24 (m, 2H), 8.31 (m, 2H), 11.13 (s, 1H). δ_C (400 MHz; DMSO-d_6; Me_4Si): 33.6, 53.6, 54.9, 114.8, 117.8, 121.1, 122.1, 125.3, 126.6, 127.7, 128.3, 128.9, 133.3, 133.8, 134.1, 134.5, 149.7, 156.8, 162.4, 182.7, 185.3. HRMS *m/z* (TOF MS ES$^-$) calcd for $C_{22}H_{13}N_2O_3^-$ ([M − H]$^-$), 353.0927, found, 353.0931.

Synthesis of 4-Nitro-*N*-{1-[2-(4-nitro-phenyl)-acetyl-amino]-9,10-dioxo-9,10-dihydro-anthracen-2-yl}-benzamide (3a). Using the method described above, the crude compound was purified by flash column chromatography on silica gel (9:1 dichloromethane/EtOAc) to afford a yellow solid (90%). δ_H (400 MHz; DMSO-d_6; Me_4Si): 7.89−7.95 (m, 2H), 8.11−8.15 (m, 3H), 8.19−8.21 (t, 1H, J = 8.8 Hz), 8.29−8.32 (m, 3H), 8.37 (d, 2H, J = 8.8 Hz), 8.42−8.46 (m, 3H), 10.52 (s, 1H) 10.81 (s, 1H). HRMS *m/z* (TOF MS ES$^-$) calcd for $C_{28}H_{15}N_4O_8^-$ ([M − H]$^-$), 535.0890, found, 535.0874.

Synthesis of 2-(4-Nitro-phenyl)-1*H*-anthra[1,2-*d*]imidazole-6,11-dione (3). Using the method described above, the crude compound was purified by flash column chromatography on silica gel (5:1 dichloromethane/EtOAc) to afford a yellow solid (75%). δ_H (400 MHz; DMSO-d_6; Me_4Si): 7.94 (s, 2H), 8.14 (d, 1H, J = 8.0 Hz), 8.19 (d, 1H, J = 8.0 Hz), 8.25 (s, 2H), 8.39 (d, 2H, J = 8.0 Hz), 8.71 (d, 2H, J = 8.0 Hz), 13.43 (s, 1H). δ_C (400 MHz; DMSO-d_6; Me_4Si): 117.8, 122.4, 123.6, 125.8, 125.2, 126.1, 127.9, 133.2, 133.3, 133.6, 134.5, 143.0, 146.3, 146.7, 155.8, 171.3, 179.7, 183.2, 183.5, 185.8. HRMS *m/z* (TOF MS ES$^-$) calcd for $C_{21}H_{10}N_3O_4^-$ ([M − H]$^-$), 368.0671, found, 368.0672.

Acknowledgment. This work was supported by the Ministry of Education of China and National Natural Science Foundation of China (Projects 20128005, 20376010, and 20472012).

Supporting Information Available: General notes and procedures; Job plot for fluoride-**1** interaction; UV−vis spectral changes of **1** and **3** in CH_3CN solution with the addition of tetrabutylammonium hydroxide; fluorescence fluoride titration spectra of **2** in CH_3CN solution; fluoride selectivity of **1** and **3**. This material is available free of charge via the Internet at http://pubs.acs.org.

JO051766Q